Journal of Hazardous Materials 211–212 (2012) 420–426

Contents lists available at SciVerse ScienceDirect

Journal of Hazardous Materials

journal homepage: www.elsevier.com/locate/jhazmat

On the characterization of nanoparticles emitted from combustion sources related to understanding their effects on health and climate

Lee Anne Sgro [b,*], Andrea D'Anna [a], Patrizia Minutolo [b,*]

[a] Dip. di Ing. Chimica, Università di Napoli Federico II, P.le Tecchio 80, 80125 Napoli, Italy
[b] Istituto di Ricerche sulla Combustione, CNR P.le Tecchio 80, 80125 Napoli, Italy

ARTICLE INFO

Article history:
Received 27 June 2011
Received in revised form 6 October 2011
Accepted 8 October 2011
Available online 10 November 2011

Keywords:
Combustion formed nanoparticles
Organic carbon
OC model particles
Water–particle interaction
Cloud condensation nuclei

ABSTRACT

This work describes the use of well-controlled laboratory flames to produce aerosols of organic carbon (OC) as model particles representative of the OC fraction of combustion-generated particulate matter emissions in fresh exhausts. Water–particle interactions are explored in two specific cases. In the first case, particles are exposed to saturated environments and come into direct contact with liquid water by bubbling flame samples through a column of water. This case is representative of particle–liquid interactions relevant to wet removal routes by particle interception by rain or fog droplets or in biological systems covered with biological fluids composed mostly of water. In the second case, the particles are exposed to sub-saturated vapors with H_2O concentrations representative of cloud-forming atmospheres. The particles' capacity to serve as atmospheric cloud condensation nuclei (CCN) by rapid growth to droplets was measured and compared to NaCl particles, which are highly soluble particles with well known activation diameters. The results show measureable interactions with water in highly saturated conditions. However, in sub-saturated environments, no growth by water condensation was observed, and fresh emissions of OC nanoparticles are not likely to act as CCN in atmospherically relevant humidity.

1. Introduction

Particulate matter (PM) affects human and environmental health as well as the radiation balance of the atmosphere. Epidemiological studies show consistent associations between exposure to PM air pollution and a wide range of serious health problems, including increased daily mortality and reduced life expectancy [1–3]. PM affects climate both by direct scattering and absorption and, more importantly, by serving as cloud condensation nuclei, named the "indirect" climate effect [4]. Carbonaceous particles are ubiquitous products of incomplete combustion of carbon-containing fuel. Ultrafine PM smaller than 100 nm, or 0.1 μm ($PM_{0.1}$), is mainly emitted from combustion sources and is mostly composed of organic carbon (OC) [5].

Recent results imply that the specific role of the OC fraction of ultrafine PM may be important in affecting cloud formation and albedo and in explaining health effects associated with pollution. The discovery of large amounts of organics detected in atmospheric clouds/fogs suggests that OC PM in polluted atmospheres may play a major role (on par with sulphates) in affecting the structure, precipitation efficiency and albedo of clouds [6–8]. Ultrafine PM is associated with premature respiratory and cardiovascular death [9], affects heart rate variability [10,11], is more potent than fine or coarse PM in various *in vitro* toxicological assays [12–14], has a higher oxidative stress potential [15–17], and may translocate after deposition in the lung to the circulatory system and extrapulmonary organs [18]. The observations that people with obstructive lung disease receive a greater dose of ultrafine PM [19] and that the amount of ultrafine PM deposited in the lung increases with decreasing particle size [20] are consistent with a diffusion limited deposition mechanism. More specifically, the OC fraction of ultrafine PM collected from urban Los Angeles air [21] and diesel exhaust [14] appears to be causing the toxic responses in toxicological *in vitro* assays. Various toxicological studies, summarized in Table 1 of supplemental materials, show that flame-generated OC nanoparticles have similar or higher toxicological responses *in vitro* to OC extracts from PM in urban air samples and from the exhausts of vehicles and engines, both in prokaryotic and eukaryotic cells. In particular, the LD_{50} value (the dose that causes death of half of the test cells in an assay testing cytotoxicity) for flame generated OC in eukaryotic cells is on the order of 10 μg/ml for several different eukaryotic cell lines [22–25]. Stojicic reports a similar LD_{50} for OC condensates collected from the exhaust of a diesel engine

* Corresponding authors.
E-mail addresses: lasgro@yahoo.com (L.A. Sgro), minutolo@irc.cnr.it (P. Minutolo).

0304-3894/$ – see front matter © 2011 Elsevier B.V. All rights reserved.
doi:10.1016/j.jhazmat.2011.10.097

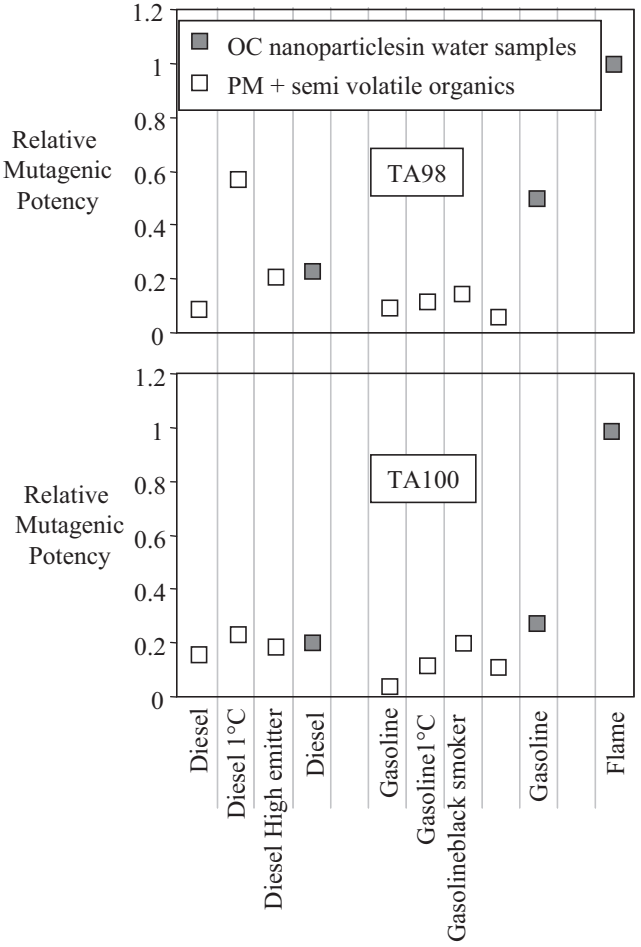

Fig. 1. Relative mutagenic potencies for organic carbon nanoparticles collected in water suspensions from flames and vehicles (solid symbols [22]) and combined PM + semi-volatile OC (open symbols [12]).

[25]. Hiura et al. report an LD_{50} about an order of magnitude higher for PM collected on filters from diesel exhaust, but they found that the refractory, black or elemental carbon fraction of these samples, was completely non-toxic after an organic fraction was removed by washing the PM with methanol [14]. Although they are on different cell lines and use different collection and testing methodologies, these results, taken together, paint a picture, which implies that the OC fraction of PM is the more toxic fraction responsible for observed toxicological responses, and the EC fraction, which accounts for a large portion of the particle mass, essentially dilutes the measured toxic potency.

Fig. 1 compares relative mutagenic potencies reported from two independent studies [12,22] that were calculated by the slope of the dose–response curve for mutagenicity measured with the same mutagenic screening assay (Ames test) on two different Salmonella Typhimurium strains, TA 98 and TA100. One study collected OC nanoparticles isolated from soot or black particles and gas phase organics from flames and vehicles. The other study collected PM on filters and semivolatile organic species extracted from cartridges downstream of the filters, and tested the mutagenic potency of PM + SVOC. Comparing the two studies, OC nanoparticles appear to have mutagenic responses similar to semivolatile organic extracts + PM collected from filters. The mutagenic potency of flame generated OC nanoparticles is 1.5–5 times higher than that of particles collected from vehicle exhausts, which implies that the vehicle samples contained relatively less toxic materials.

One hypothesis to explain the higher toxicological potential of combustion generated carbonaceous macromolecules/nanoparticles with a more organic rather than black or elemental carbon structure is that their ability to catalyze the formation of reactive oxygen species (ROS) is related to free-radical species within the particle structure or adhered on its surface. The toxicological mechanism is that small particles penetrate the lung and cause oxidative stress that can overwhelm antioxidant defence mechanisms of lung parenchyma. The ROS-forming potential of diesel exhaust particles and organic extracts on these particles has been measured with non-cellular assays in the presence of a reductant, and is correlated with their toxicological potential [21,26–28]. Electron paramagnetic (EPR) spectrometry has been used to measure the presence of free-radicals, and EPR signals in combustion generated particles and organic extracts [29] are similar to those reported for semiquinone radical species in PM2.5 (particulate matter with aerodynamic diameter <2.5 μm) [29,30] and tar extracted from cigarette smoke [31].

Impacts of nanoparticles on the environment depend strongly on interactions between particles and water in the vapor or liquid phase. Particle interactions with H_2O critically affect transportation, storage and the general fate of PM in the atmosphere and ecological systems. The hygroscopic nature of PM and its various components also critically affect particle deposition and translocation within and beyond the human respiratory system as well as sample stability, dispersion, and dose delivery in cell culture mediums and *in vitro* work.

Various forms of carbon particles can be produced by combustion synthesis. The most widely studied form of PM produced by hydrocarbon combustion is soot, which contributes to the black or elemental fraction of atmospheric carbon. By controlling combustion parameters, also other forms of carbon may be produced, such as tar-like organic compounds, fullerenes, nanotubes, and graphitic or diamond structures [32–35]. Complex combustion conditions often produce aerosols composed of mixtures of various forms of carbon particles [33,36,37]. Laboratory premixed flames can be operated in controllable, repeatable conditions [37]. Depending on the operative combustion conditions, particles with different characteristics are formed; in particular it is possible to produce organic nanoparticles which are a model of the combustion-generated fraction of the atmospheric OC without the presence of soot or other carbon species with higher three dimensional order [35,37]. This flame synthesis method provides a means for studying the effect of carbonaceous PM formed in high temperature combustion reactions entirely separated from additional effects, which may be due to lube oil and metal additives also present in applied combustion systems burning complex fuels. Recently, several research studies have been conducted to characterize flame-generated OC nanoparticles [37]. These species have a broad light absorption spectrum peaked in the UV, quite similar to those reported for humic-like substances in environmental waters and soils. The fluorescence spectra present bands typical of aromatic moieties with 1–4 rings [37], time-resolved fluorescence polarization anisotropy showed that this fluorescence is emitted by nanoparticles with a diameter of 1–3 nm [38]. The particulate nature of OC produced in flames was confirmed by the on-line measure of their size distribution function by means of differential mobility analysers (DMA) and by atomic force microscopy (AFM) [37,39]. Additionally, AFM topography has showed that such particles have a flat shape when deposited on mica plates because of their high plasticity or liquid-like structure [40].

Several works have shown that incipient OC nanoparticles generated in flames in the exhausts of vehicles and industrial burners can be isolated from gas phase OC and more graphitic soot particles. These particles also remain dispersed as stable aqueous suspensions for long periods of time (months) [22,25]. However, it

remains to ascertain whether these particles are present in solution or merely suspended in the hydrosols [37]. Also, we are aware of no prior works in the literature that have investigated interactions between water and flame-generated OC directly.

In this work, we use well-controlled laboratory flames to generate OC nanoparticles and explore their interactions with water as an interactive medium in two cases relevant for understanding the role of PM in affecting human health and the environment. In the first case, particle–liquid interactions relevant to "wet deposition" or interception of PM by rain, snow or fog in the atmosphere, and deposition on biological fluids are explored. The second case investigates particle interactions with sub-saturated vapors having H_2O concentrations representative of cloud-forming atmospheres. These measurements are a first step to determining if freshly admitted flame-generated OC PM may act as CCN.

Most of the OC particles are smaller than 10 nm, which is significantly smaller than a typical CCN "activation diameter" ($d_{activation}$), or the diameter at which 50% of the particles are activated as CCN and grow rapidly by water condensation into droplets. For example, highly soluble particles like NaCl are reported to have a $d_{activation} = 26$ nm when exposed to a humid environment with supersaturation, $S = 0.8$ [41,42]. In this work, to test the CCN-forming ability of flame-generated OC nanoparticles, we increased their size by coagulation in an undiluted section of sampling line, and measured activation curves in comparison to those for NaCl which is often used as the soluble-particle standard [41,42]. We also reduced their concentration to less than 10^4 to compare our results with earlier works reported in the literature.

2. Experimental methods

OC nanoparticles have been produced in laminar flames fueled with premixed mixture of ethylene and air. The mixture is reported in terms of equivalence ratio, i.e. the fuel/air ratio normalized by the stoichiometric one.

Particles were sampled by means of two different types of sampling systems sketched in Fig. 2. The first sampling system (Fig. 2a), collects samples of fresh flame-generated OC particulate matter by bubbling undiluted combustion products through laboratory water added to the bubbler. Undiluted products are drawn through the sampling system (bubbler/condenser) at a flow rate of 4 l/min. Combustion-generated water condenses on the cool walls of the bubbler/condenser and accumulates over time at a rate of a few ml/hour depending on the flame condition. The resulting sampled material is an aqueous dispersion of combustion products that diffuse to the bubble surface and are captured in the bubbler and those that are scrubbed out by heterogeneous condensation. Downstream of the bubbler/condenser, the sampled flow was diluted by two ejector pumps and sent to a DMA to measure throughput of particles. The overall dilution ratio of the ejector pump dilution system was 1:20, calibrated by direct flow measurement.

The second sampling system (Fig. 2b) is used to measure the size distribution of flame-generated nanoparticles with minimal sampling artifacts. It draws a small sample flow from the flame through an orifice (0.3 mm) into a much larger turbulent diluent flow of particle-free nitrogen. It has been demonstrated that this sampling system effectively suppresses particle coagulation and condensation of semivolatile species in the sampling lines when operated to achieve high dilution ratios (DR > 10^3) [43]. The dilution ratio (DR) in this probe is a function of the sample orifice, the nitrogen flow rate, and the slight underpressure in the probe drawing in the flame sample. The DR was calibrated by measuring directly CO_2 in diluted and undiluted flame products.

We performed experiments designed to measure the CCN "activation" curves of flame-generated OC nanoparticles relative to NaCl nanoparticles, for which CCN-activation curves are reported in the literature [41,42].

Flame products were drawn from an ethylene air flame operating with an equivalence ratio, $\Phi = 2.0$ and cold gas velocity = 10 cm/s. This flame produces OC particles that are mostly smaller than 10 nm [37] and we allowed them to coagulate by drawing the particles through a 6 cm long 2 mm ID tube oriented horizontally with its inlet centered 15 mm above the burner surface. In this section of sampling line, the aerosol was undiluted.

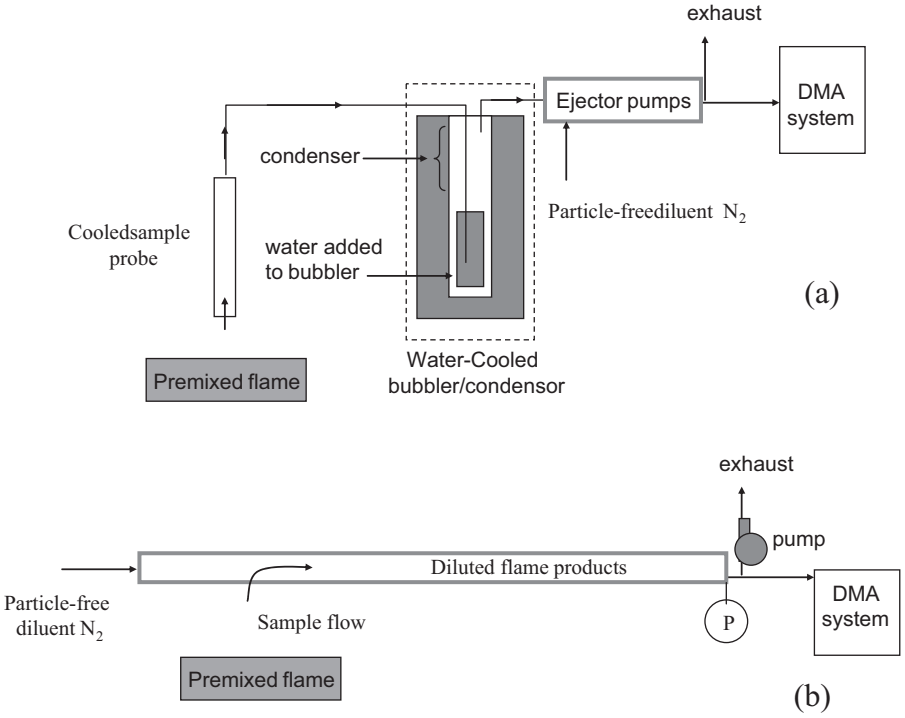

Fig. 2. Dilution systems used to sample flame-generated OC nanoparticles for testing their interactions with water.

Successive dilution occurred in an ejector pump, which created the underpressure required to draw the particles through the initial tube, and in a secondary dilution probe with variable dilution ratio (on the order of several hundred) required to reduce the particle concentration to levels that are relevant for atmospheric conditions ($\leq 10^4$ particles/cm^3).

Particles of a specific size were selected from the test aerosol with a differential mobility analyzer (TapCon 3/150 DMA). The monodisperse, size-selected aerosol flow was split to simultaneously measure the total particle concentration with a condensation particle counter (CPC, TSI model 3760A) and the fraction of particles that grow by condensation of water-vapor using an ad-hoc CPC, which operates with water as the working fluid. The TSI CPC measured the total particle concentration, N_{total}, with 100% efficiency for particles larger than 10 nm. The water-based CPC measured only those particles that grow by condensing water on their surface to a droplet with diameter larger than 300 nm, named cloud condensation nuclei (CCN). Using the nomenclature and methods reported in the literature [41,42], the results are presented as CCN-activation curves or plots of the fraction of particles that grow (CCN/N_{total}) as a function of size-selected dry particle diameter.

For comparison, we also tested NaCl particles generated with an electrospray similar to the one described by Chen et al. [44]. The NaCl particles were produced by pushing a 150 mM solution of NaCl in bidistilled laboratory water through a 30 μm silica capillary with a sharpened, uncoated tip. The capillary tip faced a metal plate with a 1 mm hole used to eliminate satellite drops and their dried residues. A voltage difference ranging from about 4.2 to 4.5 kV was applied directly to the spray solution and the flat plate. Carbon dioxide was used as the drying gas to avoid Corona discharge. The cone-jet stable operating modes was observed through a microscope and by measuring their output currents [44].

The water-based CPC is a turbulent-mixing type CPC, which exposes incoming aerosols to a vapor concentration by mixing the incoming cold aerosol flow with a hot flow issued from a saturator in a small tee. The humidified aerosol flow then travels through a growth section and droplets that are larger than 300 nm are counted at the end of the growth section by an optical particle counter (Biotest APC plus). Previous works describe in detail the design of the turbulent-mixing CPC and demonstrate its ability to grow/detect particles as small as 1 nm operating with organic working fluids [45,46]. In this work, we used water as the working fluid, and did not operate in optimal supersaturation conditions to grow all particles. Instead, we set the variable operating conditions of the CPC that determine the supersaturation in the mixing section (saturator flow, saturator temperature, and incoming aerosol temperature) to values that enabled the measurement of CCN-activation curves of NaCl particles generated by electrospray with the same size of combustion-generated particles. It is not easy to measure or infer S in the mixing section of the CPC since the temperature distribution within the mixing tee of the CPC is complex and not measured. Our approach was to measure CCN-activation curves for NaCl at fixed operating conditions in the CPC. From our measurements we infer the supersaturation by comparison with reported activation curves for NaCl particles for various S in the literature, even though they used different particle generation methods and a thermal diffusion-type CCN counter (model M-1 of DH Associates) [41,42].

3. Results

3.1. OC–water interaction: saturated conditions

The first set of experiments was done to study interaction of OC with water in highly saturated conditions. Fig. 3 compares size distributions of flame products sampled with the dilution system in Fig. 2a downstream of a Pyrex bubbler and condenser. The size distributions were measured with or without adding 25 ml of water to the bubbler, labelled "water in bubbler" and "dry" sample line respectively. Since the sample flow through the bubbler is undiluted, combustion-generated water condenses on its cool walls and accumulates over time. The concentration of water in undiluted combustion products varies slightly with fuel:air mixture and is approximately 10–13%.

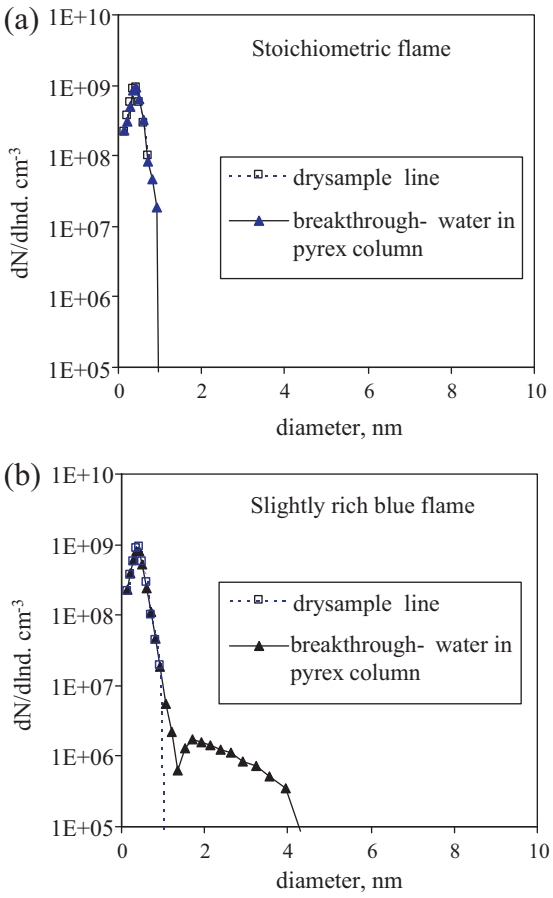

Fig. 3. Size distributions of diluted flame products sampled from a stoichiometric particle-free flame (a) compared to those measured in a slightly fuel rich, transparent blue flame (b) with either dry sampling lines (empty symbols) or by bubbling through a water column (solid symbols). All measurements taken with the system illustrated in Fig. 2b.

Size distributions were measured for a stoichiometric ($\Phi = 1$) flame (a) and a slightly fuel rich ($\Phi = 1.7$) transparent blue-colored flame (b). In all of the size distributions in Fig. 3, a sub-nanometer peak is measured, which is also measured in particle-free gasses and is mainly due to molecular clusters formed by ion-induced nucleation in the particle charger itself at ambient temperature [47]. This peak is the only one measured in the stoichiometric flame condition and remains constant with or without water in the bubbler (Fig. 3a). This result was expected since laminar premixed flames burning a stoichiometric fuel:air mixture produce only water and CO_2 and no particulate matter or gas phase products of incomplete combustion. Similarly, no particles were observed in the slightly fuel rich blue flame when the sampling line was essentially dry (Fig. 3b squares and dotted line). However, when water is added to the bubbler, a 2–4 nm mode appears in the size distribution (Fig. 3a triangles) for flame conditions $\Phi > 1.5$. These 2–4 nm species are not pure water droplets formed by homogeneous condensation or a spray mechanism in the bubbler since

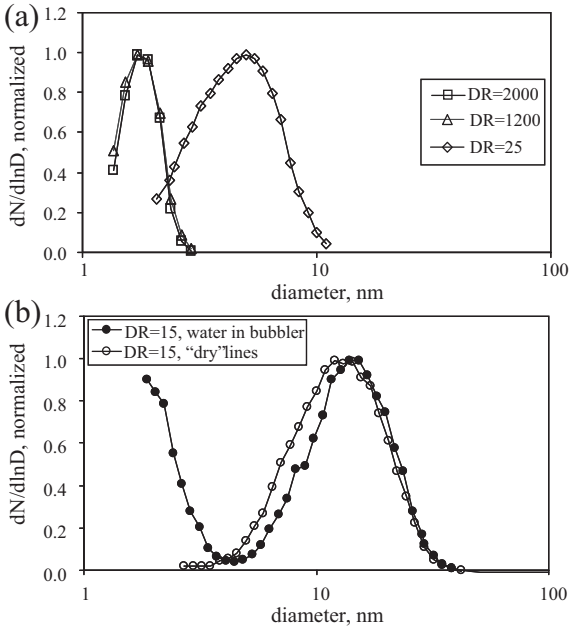

Fig. 4. Normalized size distributions measured with the dilution system illustrated in Fig. 2b(a) and a(b) with dry sample lines (empty symbols) and bubbling through a water column (solid symbols).

they are not observed when water is added to the system but the flame is off or is burning a fuel:air mixture nearer to stoichiometric conditions (Φ = 1–1.5). Consequently, we can conclude that in fuel rich Φ = 1.5–1.8 blue flames, bubbling the sample flow through water "activates" droplet formation on combustion products that serve as condensation nuclei. Furthermore, the observation that the combustion-generated condensation nuclei are not observed in the condition of a dry sample indicates that their size is smaller than 1 nm; thus, they cannot be measured due to the strong interfering signal of molecular clusters generated in the particle charger or are below the instrumental detection limit.

For the rest of the figures in this work, we report only data relevant to flame-generated particles and eliminate the sub-nanometer data.

Further increase of the fuel:air ratio produces larger particles in higher concentration so that particles are detected also with the "dry sample line". Fig. 4 plots size distributions measured in a rich flame with faint orange light emission (Φ = 1.9) using the two different dilution systems illustrated in Fig. 2. Immediate and high dilution obtained with the set up of Fig. 2b, effectively suppresses particle coagulation and heterogeneous condensation in the sample lines so that the form of the size distribution does not vary with DR ≥ 1200 (squares and triangles in Fig. 4a). When particle growth in the sample lines is effectively suppressed, the size distribution measured gives the true size of particles at the sampling point [43,47]. At lower dilution levels, DR < 1000, particle growth processes in the sample line cause the size distribution to widen and shift toward larger sizes. The relative humidity in the sampling system of Fig. 2b is approximately equal to that of combustion products (∼10%) divided by the DR, which is quite low (less than 1% even for the lowest DR). As a result, particle growth observed in the lowest dilution case (DR = 25) is due to particle coagulation and condensation of combustion products on particle surfaces and not water condensation.

Instead, with the sampling set up of Fig. 2a the dilution gasses are introduced 10 cm downstream of the bubbler/condenser system. As a result, rapid particle growth occurs in the initial undiluted section of the sampling system where concentrations of particles and semivolatile/volatile species that may condense on their surfaces are high. With this set up and DR = 15, particles in the size range 5–35 nm are measured both with and without water in the bubbler (Fig. 4b). When the sample flow is bubbled through bidistilled water added to this sampling system, a significant amount of species smaller than 4 nm is also present in the size distribution that is not observed in the case of "dry" lines without adding water to the bubbler (Fig. 4b). The size distribution of these d < 4 nm has a similar form to the one observed in the blue flame condition of Fig. 3b. The d < 4 nm species measured when bubbling combustion products through a column of water are thought to be flame-generated species with sizes lower than DMA detection limit, that grow to detectable sizes (>1 nm) by condensational growth in the saturated sampling system. Water addition to the sampling line also results in an observable growth of particles larger than 5 nm, which are shifted toward larger diameters (solid circles) compared to the size distribution measured with "dry sampling lines" (empty circles).

The combined results of Figs. 3 and 4b show that flame-generated OC nanoparticles effectively interact with water since noticeable growth is observed when water is added to the sampling lines compared to the "dry sampling lines" case. A slight but detectable increase in particle size is observed when combustion products were drawn through water added to the bubbler (Fig. 4b). Also, a "new" inception mode is observed when water is added to the sampling line that is not observed by on-line DMA without water addition to the sampling system (Figs. 3b and 4b) for flame conditions with Φ > 1.5, and this mode appears to be due to sub-nanometer combustion products that act as condensation nuclei.

Since OC particles effectively interact with water, and remain dispersed in water samples, as discussed in Section 1, we performed some tests to investigate their ability to act as CCN in less saturated conditions, representative of atmospheric conditions in cloud-forming environments.

3.2. CCN testing of flame-generated OC and electrospray-generated NaCl nanoparticles

To test the CCN-forming potential of fresh combustion-generated OC, OC nanoparticles were collected from a C/O = 0.67 flame using the sampling system depicted in Fig. 2a without the dilution system to allow particle growth. Monodisperse particles were then selected by a DMA. The value of particle concentration was chosen to avoid particle–particle interaction while studying particle–vapor interactions. Similar particle concentrations are used in the CCN-activation studies reported in the literature. Electrospray-generated NaCl particles were also used as a calibration standard to ensure that the experimental set up for measuring activation curves effectively grows soluble particles by comparison with activation curves reported in the literature using commercially available cloud condensation nucleus counters.

The calibration test was performed by selecting monodisperse NaCl particles at the exit of the DMA. Particle concentration was changed by varying the spray from the stable operating condition of cone-jet mode by reducing the electrospray voltage, and then increasing it back to the original value corresponding to stable cone-jet mode. The concentration of particles that grow to droplets larger than 300 nm, or CCN activated by condensation of water vapor, changed simultaneously with the concentration of total particles (N_{total}), but the fraction of CCN/N_{total} was constant within experimental uncertainties. Almost all of the particles were activated by water condensation in the case of 35 nm NaCl particles while only about 10% grew in the case of 25 nm NaCl particles.

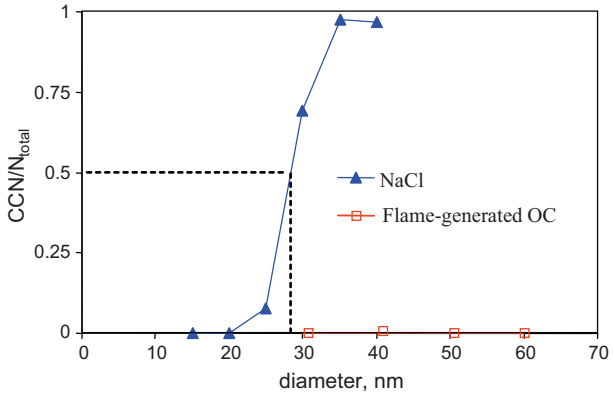

Fig. 5. Fraction of total dry test particles that grow by condensation of water vapor on their surface to lager than 300 nm as a function of the diameter of the monodisperse test particle.

The average value of the fraction of activated CCN/N_{total} from repeated measurements was used to generate an activation curve as a function of the particle diameter of the test aerosol.

Fig. 5 shows the fraction of CCN/N_{total} or particles activated by water condensation divided by the total concentration of dry particles plotted as a function of the particle diameter of the test aerosol selected by the DMA. The CCN-activation curve measured for NaCl particles is zero for particles smaller than 20 nm, has a steep increase for particles larger than 25 nm, and nearly all particles larger than 35 nm are activated. The activation diameter for which 50% of the dry particles tested grew by condensation to droplets larger than 300 nm was $d_{activation}$ = 28 nm. This result agrees well with activation diameters reported in the literature that were measured with a thermal diffusion-type CCN chamber [41,42] operating with S = 0.8, which is a good estimate of the saturation environment causing condensation in our experiment.

For the same experimental settings, changing only the particle source from the electrospray source to diluted combustion products, we observed no activation by water condensation even for particles as large as 60 nm with concentrations similar to that of the same size NaCl particles. We also increased the flow rate and/or the temperature of the saturator in the water-based CPC in order to increase S. Even under such conditions, we observed no significant particle growth prior to homogeneous nucleation of droplets. The conditions necessary to obtain homogeneous nucleation were checked by setting the voltage applied to the DMA to zero so that no particles were allowed to reach the DMA exit and the CPC.

4. Discussion and conclusions

In this work we have studied interaction with water of OC nanoparticles produced in flame as model particle of OC emitted in atmosphere by combustion systems.

In particular, particle–water interactions were studied under highly saturated conditions, which are representative of particle–liquid interactions relevant to wet removal routes, by particle interception by rain or fog droplets or in biological systems covered with biological fluids composed mostly of water. In a second case, the particles were exposed to sub-saturated vapors with H_2O concentrations representative of cloud-forming atmospheres, and the particles' capacity to serve as atmospheric CCN by rapid growth to droplets was measured and compared to NaCl particles as a standard. The results have shown measureable interactions with water in highly saturated conditions. However, in sub-saturated environments, no growth by water condensation was observed, and fresh emissions of OC nanoparticles are presumably not likely to act as CCN in atmospherically relevant humidity.

The lack of significant particle growth observed for flame-generated OC in this study is consistent with results reported in the literature for diesel exhaust particles that measured low or negative growth factors in humidity conditions similar to the ones investigated in this study ($S \sim 0.8$) [48]. In spite of the results presented here, the question remains whether combustion-generated OC PM significantly affect cloud formation in the presence of other substances with known water solubility like sulphates and NaCl. It remains to be verified if particle transformation under atmospheric conditions, including exposure to UV radiation and oxidation, may significantly increase the CCN forming potential of flame-generated OC.

The indication from toxicological studies that the OC fraction of PM appears to be more potent than the BC fraction collected from urban atmospheres and combustion exhausts (see introduction) is interesting and warrants further study. More specifically, the observation that a somewhat polar fraction of OC that can be removed with methanol can render the washed PM totally non-toxic is relevant to the results/observations presented in this paper. The OC fraction collected in water remains as a stable dispersion for relatively long time periods (months). By contrast, black carbon, produced in soot-forming flame conditions and sampled in water with the same procedure, quickly settles or migrates to the borders of water suspensions within minutes to several hours depending on the sample [22,25]. Centrifugation designed to separate particles larger than 10 nm results in the removal of black particles from flame-generated PM samples in water suspensions without changing significantly either the total organic carbon concentration or the toxicological potency of the samples [25]. Another interesting observation is that stable dispersions of OC particles in bidistilled water aggregate when cell culture medium or proteins are added [22]. In *in vitro* toxicological assays testing complex mixtures of PM, it is quite challenging to understand the actual delivered dose and the characteristics of particles and particle–protein aggregates after they are administered to the cell medium. Flames offer a repeatable and controllable combustion source for particle generation of carbonaceous nanoparticles with specific properties (size, aggregation state, degree of order and graphitization, etc.).

Acknowledgement

The authors wish to thank MSE-CNR project on "Carbone Pulito" for financial support.

Appendix A. Supplementary data

Supplementary data associated with this article can be found, in the online version, at doi:10.1016/j.jhazmat.2011.10.097.

References

[1] C.A. Pope, M. Ezzati, D.W. Dockery, Fine-particulate air pollution and life expectancy in the United States, N. Engl. J. Med. 360 (2009) 376–386.
[2] B. Brunekreef, S.T. Holgate, Air pollution and health, Lancet 360 (2002) 1233–1242.
[3] R.D. Brook, B. Franklin, W.E. Cascio, Y. Hong, G. Howard, M. Lipsett, R.V. Luepker, M.A. Mittleman, J.M. Samet, S.C.J. Smith, I.B. Tager, Air pollution and cardiovascular disease: a statement of the health care professionals from the expert panel on population and prevention science of the American Heart Association, Circulation 109 (2004) 2655–2671.
[4] J.H. Seinfeld, S.N. Pandis, Atmospheric Chemistry and Physics: From Air Pollution to Climate Change, J. Wiley, New York, 1998.
[5] G.R. Cass, L.A. Hughes, P. Bhave, M.J. Kleeman, J.O. Allen, L.G. Salmon, The chemical composition of atmospheric ultrafine particles, Philos. Trans. R. Soc. Lond. A 358 (2000) 2581–2592.
[6] T. Novakov, J.M. Penner, Large contribution of organic aerosols to cloud-condensation-nuclei concentrations, Nature 365 (1993) 823–826.

[7] V. Ramanathan, P.J. Crutzen, J.T. Kiehl, D. Rosenfeld, Aerosols, climate, and the hydrological cycle, Science 294 (2001) 2119–2124.
[8] S. Fuzzi, M.C. Facchini, S. Decesari, E. Matta, M. Micrcea, Soluble organic compounds in fog and cloud droplets: what have we learned in the past few years? Atmos. Res. 64 (2002) 89–98.
[9] A. Peters, H.E. Wichmann, Health effects of fine and ultrafine particles: the Erfurt studies, Epidemiology 13 (2002) 255.
[10] K.J. Chuang, C.C. Chan, T.C. Su, L.Y. Lin, C.T. Lee, Associations between particulate sulphate and organic carbon exposures and heart rate variability in patients with or at risk for cardiovascular diseases, J. Occup. Environ. Med. 49 (2007) 610–617.
[11] J.M. Samet, A. Rappold, D. Graff, W.E. Cascio, J.H. Berntsen, Y.T. Huang, M. Herbst, M. Bassett, T. Montilla, M.J. Hazucha, P.A. Bromberg, R.B. Devlin, Concentrated ambient ultrafine particle exposure induces cardiac changes in young healthy volunteers, Am. J. Respir. Crit. Care Med. 179 (2009) 1034–1042.
[12] J.C. Seagrave, J.D. McDonald, A.P. Gigliotti, K.J. Nikula, S.K. Seilkop, M. Gurevich, J.L. Mauderly, Mutagenicity and in vivo toxicity of combined particulate and semivolatile organic fractions of gasoline and diesel engine emissions, Toxicol. Sci. 70 (2002) 212–226.
[13] V. Castranova, J.Y.C. Ma, H.M. Yang, J.M. Antonini, L. Butterworth, M.W. Barger, J. Roberts, J.K.H. Ma, Effect of exposure to diesel exhaust particles on the susceptibility of the lung to infection, Environ. Health Perspect 109 (2001) 609–612.
[14] T.S. Hiura, M.P. Kaszubowski, N. Li, A. Nel, Chemicals in diesel exhaust particles generate reactive oxygen radicals and induce apoptosis in macrophages, J. Immunol. 163 (1999) 5582–5591.
[15] T. Xia, M. Kovochich, J. Brant, M. Hotze, J. Sempf, T. Oberley, C. Sioutas, I.Y. Yeh, M.R. Wiesner, A.E. Nel, Comparison of the abilities of ambient and manufactured nanoparticles to induce cellular toxicity according to an oxidative stress paradigm, Nano Lett. 6 (2006) 1794–1807.
[16] H. Yang, C. Liu, D. Yang, H. Zhang, Z. Xi, Comparative study of cytotoxicity, oxidative stress and genotoxicity induced by four typical nanomaterials: the role of particle size, shape and composition, J. Appl. Toxicol. 29 (2008) 69–78.
[17] N. Li, M. Hao, R.F. Phalen, W.C. Hinds, A.E. Nel, Particulate air pollutants and asthma. A paradigm for the role of oxidative stress in PM-induced adverse health effects, Clin. Immunol. 109 (2003) 250–265.
[18] A. Peters, B. Veronesi, L. Calderón-Garcidueñas, P. Gehr, L.C. Chen, M. Geiser, W. Reed, B. Rothen-Rutishauser, S. Schürch, S. Holger, Translocation and potential neurological effects of fine and ultrafine, Part. Fibre Toxicol. 3 (2006) 13.
[19] J.S. Brown, K.L. Zeman, W.D. Bennett, Ultrafine particle deposition and clearance in the healthy and obstructed lung, Am. J. Respir. Crit. Care Med. 166 (2002) 1240–1247.
[20] P.A. Jaques, C.S. Kim, Measurement of total lung deposition of inhaled ultrafine particles in healthy men and women, Inhal. Toxicol. 12 (2000) 715–731.
[21] N. Li, C. Sioutas, A. Cho, D. Schmitz, C. Misra, J. Sempf, M. Wang, T. Oberley, J. Froines, A. Nel, Ultrafine particulate pollutants induce oxidative stress and mitochondrial damage, Environ. Health Perspect 111 (2003) 455–460.
[22] L.A. Sgro, A. Simonelli, L. Pascarella, P. Minutolo, D. Guarnieri, N. Sannolo, P. Netti, A. D'Anna, Toxicological properties of nanoparticles of organic compounds (NOC) from flames and vehicle exhausts, Environ. Sci. Technol. 43 (2009) 2608–2613.
[23] N. Stojicic, C. Baumstark-Khan, C.E. Hellweg, H.-H. Grotheer, G. Reitz, W. Kolanus, R. Hemmersbach, Toxicity of ethylene combustion condensates is directly proportional to their carbon content, Toxicology 269 (2010) 35–40.
[24] P. Pedata, M. Boccellino, R. La Porta, M. Napolitano, P. Minutolo, L.A. Sgro, F. Zei, N. Sannolo, L. Quagliuolo, Interaction between combustion-generated organic nanoparticles and biological systems: *in vitro* study of cell toxicity and apoptosis in human keratinocytes, J. Nanotoxicol. (2011), doi:10.3109/17435390.2011.579630.
[25] N. Stojicic, Toxicity of combustion condensates on human cells, Ph.D. Dissertation, Faculty of Natural Sciences, Rheinische Friedrich-Wilhelms University, Bonn, Germany, 2009.
[26] C.F.A. Vogel, E. Sciullo, P. Wong, P. Kuzmicky, N. Kado, F. Matsumura, Induction of proinflammatory cytokines and C-reactive protein in human macrophage cell line U937 exposed to air pollution particulates, Environ. Health Perspect 113 (2005) 1536–1541.
[27] C.-J. Pan, D.A. Schmitz, A.K. Cho, J. Froines, Inherent redox properties of diesel exhaust particles: catalysis of the generation of reactive oxygen species by biological reductants, Toxicol. Sci. 81 (2004) 225–232.
[28] Y.Y. Kumagai, N. Shimojo, Induction of oxidative stress and dysfunction of nitric oxide-dependent vascular tone caused by quinones contained in diesel exhaust particles, J. Health Sci. 47 (2001) 439–445.
[29] B. Dellinger, W.A. Pryor, R. Cueto, G.L. Squadrito, V. Hegde, W.A. Deutsch, Role of free radicals in the toxicity of airborne fine particulate matter, Chem. Res. Toxicol. 14 (2001) 1371–1377.
[30] S. Balakrishna, S. Lomnicki, K.M. McAvey, R.B. Cole, B. Dellinger, S.A. Cormier, Environmentally persistent free radicals amplify ultrafine particle mediated cellular oxidative stress and cytotoxicity, Part. Fibre Toxicol. 6 (2009), doi:10.1186/1743-8977-6-11.
[31] K. Stone, E. Bermudez, L.Y. Zang, K.M. Carter, K.E. Queenan, W.A. Pryor, The ESR properties, DNA nicking, and DNA association of aged solutions of catechol versus aqueous extracts of tar from cigarette smoke, Arch. Biochem. Biophys. 319 (1995) 196–203.
[32] J.B. Howard, J.T. McKinnon, Y. Makarovsky, A.L. Lafleur, M.E. Johnson, Fullerenes C60 and C70 in flames, Nature 352 (1991) 139–141.
[33] C.D. Lagally, C.C.O. Reynolds, A.P. Grieshop, M. Kandlikar, S.N. Rogak, Carbon nanotube and fullerene emissions from spark-ignited engines, Aerosol Sci. Technol. 46 (2012) 156–164, doi:10.1080/02786826. 2011.617399.
[34] W. Merchan-Merchan, A.V. Saveliev, L. Kennedy, W.C. Jimenez, Combustion synthesis of carbon nanotubes and related structures, Prog. Energy Combust. Sci. 36 (2010) 696–727.
[35] P. Minutolo, G. Rusciano, L.A. Sgro, G. Pesce, A. Sasso, A. D'Anna, Surface enhanced Raman spectroscopy (SERS) of particles produced in premixed flame across soot threshold, Proc. Combust. Inst. 33 (2011) 649–657.
[36] Z. Su, W. Zhou, Y. Zhang, New insight into the soot nanoparticles in a candle flame, Chem. Commun. 47 (2011) 4700–4702.
[37] A. D'Alessio, A. D'Anna, P. Minutolo, L.A. Sgro, Nanoparticles of organic carbon (NOC) formed in flames and their effects in urban atmospheres, in: H. Bockhorn, A. D'Anna, A.F. Sarofim, H. Wang (Eds.), Combustion Generated Fine Carbonaceous Particles, Karlsruhe University Press, Karlsruhe, 2009, pp. 205–230.
[38] A. Bruno, F. Ossler, C. de Lisio, P. Minutolo, N. Spinelli, A. D'Alessio, Detection of fluorescent nanoparticles in flame with femtosecond laser-induced fluorescence anisotropy, Opt. Express 16 (2008) 5623–5632.
[39] L.A. Sgro, A. De Filippo, G. Lanzuolo, A. D'Alessio, Characterization of nanoparticles of organic carbon (NOC) produced in rich premixed flames by differential mobility analysis, Proc. Combust. Inst. 31 (2007) 631–638.
[40] A.C. Barone, A. D'Alessio, A. D'Anna, Morphological characterization of the early process of soot formation by atomic force microscopy, Combust. Flame 132 (2003) 181–187.
[41] C.E. Corrigan, T. Novakov, Cloud condensation nucleus activity of organic compounds: a laboratory study, Atmos. Environ. 33 (1999) 2661–2668.
[42] C.N. Cruz, S.N. Pandis, A study of the ability of pure secondary organic aerosol to act as cloud condensation nuclei, Atmos. Environ. 31 (1997) 2201–2214.
[43] L.A. Sgro, A. D'Anna, P. Minutolo, Charge fraction distribution of nucleation mode particles: new insight on the particle formation mechanism, Combust. Flame 158 (2011) 1418–1425.
[44] D.-R. Chen, D.Y.H. Pui, S.L. Kaufman, Electrospraying of conducting liquids for monodisperse aerosol generation in the 4 nm–1.8 μm diameter range, J. Aerosol Sci. 26 (1995) 963–977.
[45] L.A. Sgro, J. Fernández de la Mora, A simple turbulent mixing CNC for charged particle detection down to 1.2 nm, Aerosol Sci. Technol. 38 (2004) 1–11.
[46] C.S. Kim, K. Okuyama, J. Fernández de la Mora, Performance evaluation of an improved particle size magnifier (PSM) for single nanoparticle detection, Aerosol Sci. Technol. 37 (2003) 791–803.
[47] L.A. Sgro, A. D'Anna, P. Minutolo, Charge distribution of incipient flame-generated particles, Aerosol Sci. Technol. 44 (2010) 651–662.
[48] E. Weingartner, H. Burtscher, U. Baltensperger, Hygroscopic properties of carbon and diesel soot particles, Atmos. Environ. 31 (1997) 2311–2327.